Mechanics of Materials 184 (2023) 104752

Contents lists available at ScienceDirect

Mechanics of Materials

journal homepage: www.elsevier.com/locate/mechmat

Research paper

Strain sensitivity and microscopic deformation mechanism of graphene foam containing active nanoparticles under magnetic fields

Muhammad Bilal Khan [a,*], Chao Wang [c,e], Shuai Wang [d], Shaohua Chen [b,**]

[a] Faculty of Mechanical Engineering, Ghulam Ishaq Khan Institute of Engineering Sciences and Technology, Topi, Swabi, 23640, KP, Pakistan
[b] Institute of Advanced Structure Technology, Beijing Institute of Technology, Beijing, 100081, China
[c] LNM, Institute of Mechanics, Chinese Academy of Sciences, Beijing, 100190, China
[d] School of Mechanical and Electrical Engineering, Beijing University of Chemical Technology, Beijing, 100029, China
[e] School of Engineering Science, University of Chinese Academy of Sciences, Beijing, 100049, China

ARTICLE INFO

Keywords:
Magnetic aerogel
External field
Strain sensitivity
Micro deformation mechanism
Coarse-grained molecular dynamics

ABSTRACT

Magnetic aerogels have attracted many practical applications in recent years, which requisites a comprehensive understanding on basic mechanics of this hybrid composite system. In this paper, the microscopic deformation mechanism and strain variation (ε_Δ) of such a hybrid material under external magnetic field (E_f) is systematically studied by the coarse-grained molecular dynamics simulation method. The major factors like layer thickness, magnitude of external magnetic field and crosslinks effects are mainly considered. The recovery behavior is also studied under cyclic E_f. Interestingly, the ε_Δ of such a hybrid material is much affected by the graphene sheet thickness, magnitude of applied E_f and crosslinks, due to their direct influences on the microstructural evolution. The ε_Δ of non-bonded hybrid composite with single layer thick graphene sheet ($\varepsilon_\Delta \sim 0.19$) is four times higher relative to eight layers thick system ($\varepsilon_\Delta \sim 0.045$). With the increase of graphene sheet thickness, the microstructural evolution of nanoparticles will change from wrapping of single layer sheets around them to flow and jump from one thick sheet to other. We also found the critical value of E_f, i.e., 200 nN for single layer thick graphene sheet hybrid systems beyond which the ε_Δ tend to decrease, however, ε_Δ for eight layers system continue to increase as a function of E_f magnitude. The addition of crosslinks remarkably enhances the ε_Δ (~ 0.74) and recovery ($\sim 90\%$) of hybrid composite system. The bonded nanoparticles initiate the folding and unfolding mechanism of graphene sheets during cyclic E_f. The results clarify the micro mechanism and basic mechanics of magnetic aerogels that will be helpful to the design the future devices and advanced sensors.

1. Introduction

Three dimensional graphene foam has proved to be as an exceptional material based upon distinctive properties of having super elasticity (Wang et al., 2019a), ultralow density (Samad et al., 2015), adequate conductivity (Chen et al., 2014), high surface area (Xu et al., 2019) and most importantly the higher tendency of accommodating other materials (as fillers) within their matrix which make them applicable to diverse potential fields like strain sensors, super capacitor electrodes, and shock damping (Shah et al., 2021; Pierre and Pajonk, 2002; Suktha et al., 2019).

The inclusion of magnetic materials in aerogels leads to advanced composite material termed as magnetic aerogel (Shah et al., 2021). The magnetic nanoparticles inclusion can be achieved through dispersion, coating and growth in solutions followed by the various drying steps like pressure or freeze drying opted based upon desired applications (Shah et al., 2021). These magnetic aerogels owing responsive and active nanoparticles have attracted significant attention because of extraordinary electronic, catalytic, optical and magnetic properties. (Kharissova et al., 2015; Casula, et al., 2001; Casu et al., 2007). Sang-Heon Lee et al. (2014) reported the novel 3D network of graphene-ferromagnetic hybrid composite for fast magneto shape memory alloy applications having significant mechanical and thermal stability. Shoupu Zhu et al. (2020) anchored the magnetic iron oxide nanoparticles into graphene foam matrix for high performance electromagnetic interference shielding applications. Sudong Yang et al. (2014) also reported the magnetic

* Corresponding author.
** Corresponding author.
E-mail addresses: muhammadbilaljadoon@gmail.com (M.B. Khan), shchen@bit.edu.cn (S. Chen).

https://doi.org/10.1016/j.mechmat.2023.104752
Received 1 April 2023; Received in revised form 30 June 2023; Accepted 25 July 2023
Available online 26 July 2023

aerogel for efficient oil and various organic solvent adsorption. Furthermore, he also achieved the magnetic driven oil-water separation with greater selectivity of oil. Lee Huang et al. (2015) incorporated the Pd nanoparticles into graphene foam matrix for the synthesis of efficient magnetic and hydrogen detection sensor. Xiang Xu et al. (2015a) reported 3D graphene aerogel decorated with Fe_3O_4 nanoparticles for magnetic field sensing applications, capable of 52% reversible magnetic field induced strain. M. Husnain Zaib et al. (Zeb et al., 2019) fabricated the graphene foam/metal sulphide nanocrystals device that elevated the magnetoresistance up to 130% at room temperature against 5T induced magnetic field strength as a results of the induced nanocrystals. Can Liu et al. (2015) synthesized the magnetic aerogel (Fe_3O_4/Graphene Foam) for oil-water separation application.

Magnetic aerogels have become the advanced multifunctional emerging materials based upon its diversified applications. However, they are still in embryonic stage and many challenges need to be addressed. The thorough comprehension of magnetic aerogel mechanics is linked to the conception of particles arrangements, movement and particle–sheets interaction under applied magnetic field, that will lead to the further improvement in design and performance of magnetic aerogels (Li et al., 2020a). Gao wei et al. (Gao and Wang, 2019) attempted to investigate the particle size combination on magneto-mechanical properties of magnetorheological elastomers. The varying particle size combination showed negligible effect on magnetic properties, the highest mechanical properties could be achieved at optimal mixture ratio of 1:2 for medium to small particles at fixed mass ratio of large size particles. However, the microstructural deformation and basic mechanics like particles-sheet interaction, particles movements still need to be examined for better understanding of such an auspicious composite system. To our best knowledge, no one have specifically reported the numerical model of magnetic aerogels, subjected to magnetic or any external field. Nanoparticles and graphene sheet interaction under magnetic field in still unclear, which can be key factor to understand basic mechanics of magnetic aerogel systems.

In this work, CGMD simulations are performed as numerical experiments to orderly investigate the strain variation, recovery behavior and the corresponding micro deformation mechanism of particle-filled graphene foam materials under external magnetic field (E_f) applied on active nanoparticles only. The particles movements, particles-sheet interaction and folding-unfolding of graphene sheets have been clearly divulged as a function of graphene sheet thickness, crosslink density and applied field magnitude. These results could not only enhance fundamental understanding, but also obliging for better design of future magnetic aerogels materials.

2. Numerical model of GrFs contained-NPs

2.1. Mesoscopic coarse-grained method

We not only endorse but also extensively applied the Cranford and Buehler (2011) proposed coarse-grained model to study the deformation mechanisms and mechanical properties of both graphene and pure GrFs (Wang et al., 2018a, 2019b; Liu et al., 2018; Pan et al., 2017, 2018; Shang et al., 2018). In this model, a single coarse-grained bead represents the 2.5 × 2.5 nm^2 graphene sheet and connection of beads equivalent to large piece of graphene layer is achieved through linear and angle springs. The potential energy of linear springs among bonded beads is described by $\varphi_P = k_P(r-r_0)^2/2$, where k_P and r are the spring constant and the distance between two bonded beads with an equilibrium distance $r_0 = 2.5$ nm, respectively. The equation $\varphi_\varphi = k_\varphi(\varphi-\varphi_0)^2/2$ is used to evaluate the potential energy of in-plane springs, where k_φ denotes the spring constant related to the bending angle φ among three beads with a referenced equilibrium angle $\varphi_0 = 90^\circ$. The potential energy of out-of-plane angle springs is denoted by $\varphi_\theta = k_\theta(\theta\text{-}\theta_0)^2/2$ with a spring constant k_θ, where θ denotes the bending angle among three beads with a referenced equilibrium value $\theta_0 = 180^\circ$. The Lennard-Jones potential $\varphi = 4\varepsilon((\sigma/r)^{12}\text{-}(\sigma/r)^6)$, is used for the van der Waals interaction between neighbor beads (NPs and/or graphene sheets) with different values of ε and σ, where ε, σ and r is the depth of potential well, the zero-energy distance and the bead-to-bead distance, respectively. For clarity, we distinguished the beads type through subscript, i.e., ε_n and σ_n for NP beads, ε_g and σ_g for graphene sheets beads, ε_{ng} and σ_{ng} for beads between NPs and graphene sheets. In all our simulations, $\varepsilon_p = \varepsilon_{ng} = \varepsilon_g$ is set for simplicity. ε_g and σ_g for graphene sheets is obtained based on the equivalent energy principle and given in Table S1.

2.2. Numerical fabrication of GrFs contained-NPs

The two-step method aligned with experimental approach (Wang et al., 2018b) is opted for the creation of our numerical NPs-contained GrF model: first, a pure GrF without NPs is assembled by randomly distributed 100 square CG sheets (the side length of 50 nm) in a box having length, width and height about 178 nm, 180 nm and 170 nm, respectively. For section 3.2, i.e., the crosslink density effect, a certain amount of crosslinks with respect to existing bonds are also added to connect the neighbor sheets into the as-synthesized pure GrF similar to the strong physical adhesion or chemical bonds (i.e., chemical groups) in practical systems (Chen et al., 2020), and the potential energy of crosslinks is stated by the harmonic function $\varphi_c = k_c(r-r_{c0})^2/2$ as well as that for the linear spring in bonded beads, where k_c, r_{c0} and r is the spring constant, the equilibrium and current length of crosslinks, in all our simulations, $k_c = k_s$ and $r_{c0} = r_0 = 2.5$ nm. In the second step, a desired volume fraction of NPs are randomly intercalated into the porous structure of the as-synthesized pure GrF, later an equilibrium simulation is conducted to attain a stable and well-equilibrated state of NPs-contained GrFs, showing total energy fluctuation less than 1% as shown in Fig. S1 Our numerical model density range is 180–240 mg/cm^3, which is consistence with the experimentally reported density range of 12–280 mg/cm^3 (Kang et al., 2020; Shi et al., 2019; Li et al., 2020b). The relative density of our model is ~8.9% corresponding to the porosity of 91.1%. A single sheet in real materials usually comprise of 1–10 graphene layers (Nieto et al., 2015; Chen et al., 2011; Dienwiebel et al., 2004). In our numerical model, we willingly opted the 1,4, and 8 layered sheets as per requirement, however the detailed study related to sheet layers effect in pure graphene foams system can be found in our previous work (Wang et al., 2016).

2.3. Simulation of external magnetic fields

The direct magnetic field function cannot be used in numerical experiments due to limitation of MD simulation. Therefore, we extract the force experienced by nanoparticles under applied magnetic field in experimentation through expression (Brown and L.J.J.o.A.P. Flax, 1964) $F = \pi R^2B^2/2\mu_0(\mu_m/\mu_0\text{ -1})$, where B is magnetic field used in experiments, R is solenoid radius in nm for our model dimensions and μ_0, μ_m are the magnetic permeabilities. The force magnitude generated by experimentally applied uniform magnetic field range i. e 0.1–1.2T is in range of ~10–1000 nN (Xu et al., 2015b). Analogous to experiments (Xu et al., 2015b), the nanoparticles were subjected to uniaxial external force (E_f) along non-periodic boundary (y-axis) in numerical experimentation. The force range applied on nanoparticles is opted based upon the force magnitude generated experimentally.

The system owes both periodic (x & z-axis) and non-periodic(y-axis) boundary conditions. NPT assembly technique is adopted to deal with the system at a constant room temperature 300 K and one barometric pressure. The lower boundary of the box along y-axis is fixed using fix/wall function to mimic the real scenarios as observed in experiments (Xu et al., 2015b). A time step of 1 fs is opted. All the simulations are performed in the large-scale atomic/molecular massively parallel simulator (LAMMPS) (Plimpton, 1995). The results are visualized based on the Open Visualization Tool (OVITO) (Stukowski, 2010).

The initial state of the well-equilibrated 3D numerical model of GrFs

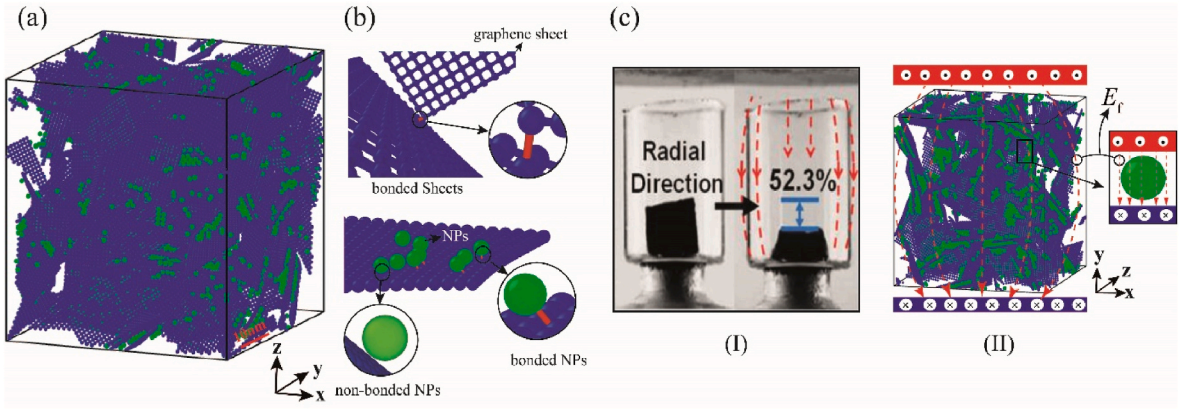

Fig. 1. Numerical model of 3D GrFs contain-NPs. (a) The initial well-equilibrated configuration of GrFs contain-NPs with NPs (green) adsorbed on the graphene sheets (blue); (b) crosslinks and nanoparticles distribution in 3D GrFs contain-NPs; graphene sheets-bonded to-graphene sheets, both bonded and non-bonded NPs distribution on graphene sheets; (c) Schematic illustration; (I) Experimental study of 3D NPs-contained GrFs under magnetic field (Xu et al., 2015b), (II) Our Numerical model of 3D GrFs contain-NPs subject to external magnetic field (E_f). (For interpretation of the references to colour in this figure legend, the reader is referred to the Web version of this article.)

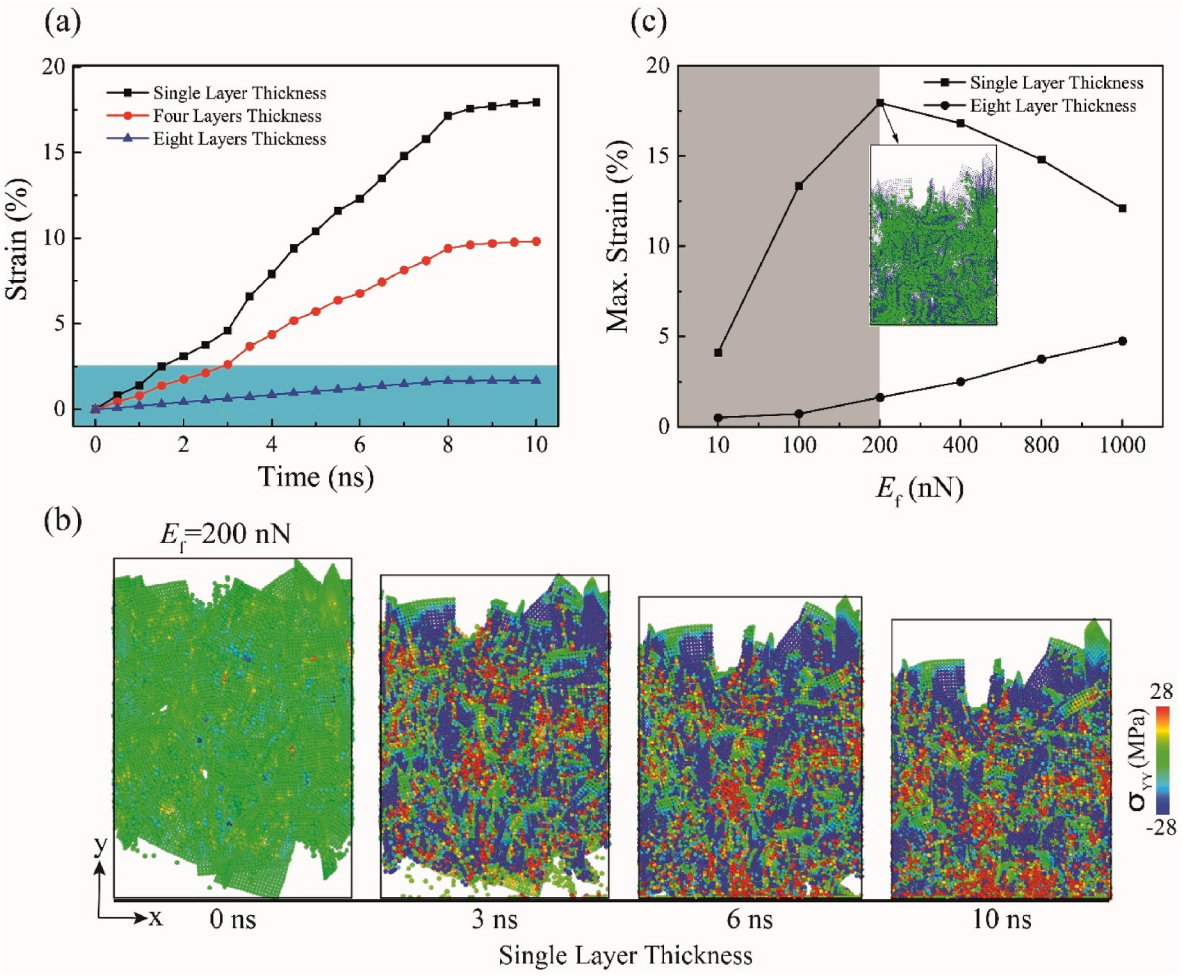

Fig. 2. The strain variation (ε_Δ) and microscopic deformation of GrFs contain-NPs system.(a) Strain variation of single, four and eight layers thick GrFs contain-NPs system at $E_f \sim 200$ nN relative to time (ns); (b) Stress distribution in single layer thick GrFs contain-NPs system at $E_f \sim 200$ nN; (c) Maximum strain of single and eight layer thick GrFs contain-NPs system as function of E_f magnitude.

contain-NPs is depicted in Fig. 1a, in which bonded graphene sheets (blue) and bonded/non-bonded NPs (green) with graphene sheets are randomly distributed as demonstrated in Fig. 1b. The bonded and non-bonded NPs particles are uniformly distributed, well consistent with experimental findings. Like experimental results (Xu et al., 2015b; Gu and Zhu, 2020; Wang et al., 2020; Zhang et al., 2020; Yuan et al., 2020), the NPs are anchored (through coupling agent) and adsorbed on surface of graphene sheets. In Fig. 1c, schematic demonstration of induced

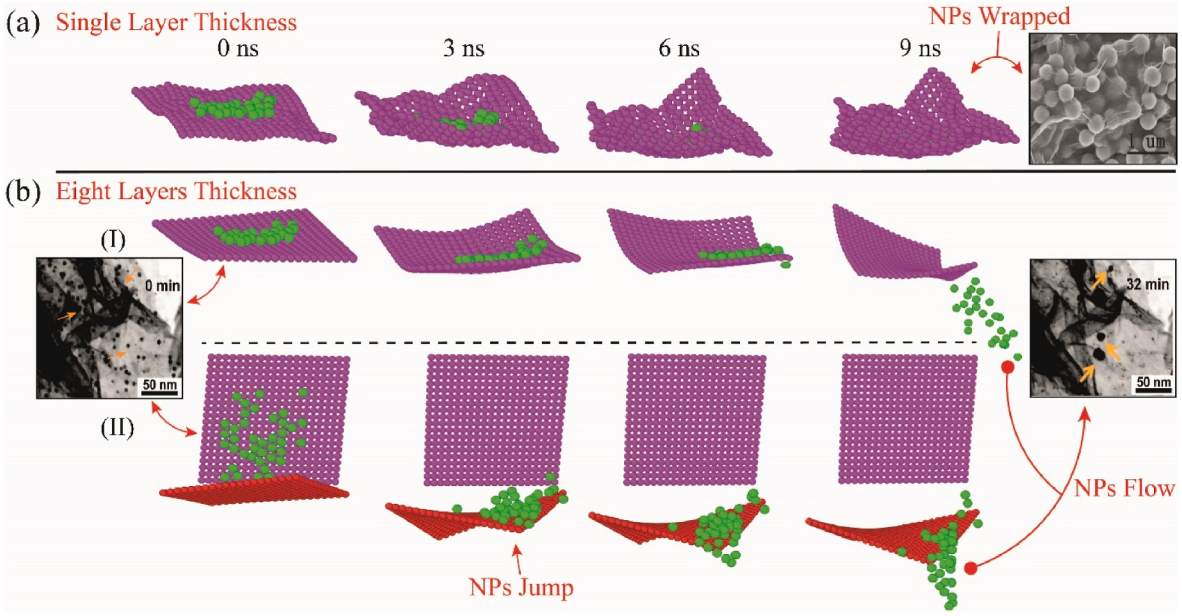

Fig. 3. Microstructural evolution of single- and eight-layers thick 3D GrFs contain-NPs system under applied E_f. (a) Single layer thick graphene sheets wrap around the NPs; similar to SEM image of wrapped graphene sheets around nano-balls (Wei et al., 2013); (b) Eight layers thick graphene sheets; (I) In plane flow of NPs on the surface of graphene sheets that eventually rushed into pores at 9 ns ; (II) Jump of NPs from one sheet (pink) to another (red) under E_f impact and eventually drain out into pores, the (I) and (II) is similar to SEM images explaining the flow of NPs across surface of graphene sheets (Jin et al., 2010). (For interpretation of the references to colour in this figure legend, the reader is referred to the Web version of this article.)

uniaxial external field in our numerical experiments mimicking to experimental setup is demonstrated. The simulations of uniaxial external field along non-periodic boundary conditions are conducted on the numerical model of GrFs contain-NPs to extract the strain-time relationship and unveil the microscopic deformation mechanisms. The lower boundary wall (y-axis) of 3D GrFs contain-NPs is fixed to generate the reaction mechanism like real scenario, otherwise NPs and sheets continue to drift uniaxially under applied E_f.

3. Results and discussions

3.1. Effect of graphene layers

Initially similar to our previous work (Khan et al., 2020), we opted the 3D GrFs contain-NPs system with volume fraction (V_f) 8% and size 3 nm of non-bonded NPs, freely adsorbed on the surface of uniformly distributed graphene sheets. We specifically expose the non-bonded adsorbed NPs to E_f systematically as a function graphene sheets thickness and, E_f magnitude. We evaluated the effect of graphene sheets thickness on strain variation of 3D GrFs contain-NPs system, Furthermore, we also investigated the effect of E_f magnitude on micro structural deformation and maximum induced strain in 3D GrFs contain-NPs system Initially, we studied the strain variation behavior of single, four- and eight-layers thick 3D GrFs contain-NPs system at constant external field ($E_f \sim 200$ nN) as shown in Fig. 2a. We found that ε_Δ of single layer thick 3D GrFs contain-NPs system increases linearly to the maximum value of $\varepsilon_\Delta \sim 18\%$ at 8 ns and eventually become stable, i.e., beyond 8 ns the system exhibits negligible strain variation, i.e., $\Delta\varepsilon_\Delta \sim 0\%$. The four layers thick system exhibits similar trend to single layer and shows strain variation value of $\varepsilon_\Delta \sim 11\%$. However, the eight layers thick 3D GrFs contain-NPs system shows insignificant ε_Δ (<2.5%) as highlighted in Fig. 2a. Therefore, we deduced that layer's thickness has significant effect on the overall deformation of 3D GrFs contain-NPs systems. The interaction of NPs and graphene sheets are much contrasting as a function of layer thickness of graphene sheets. We further demonstrated the deformation behavior of single layer thick system at $E_f \sim 200$ nN in Fig. 2b. We observed the homogeneous collapse of 3D GrFs contain-NPs system composed of single layer graphene sheets particularly. The graphene sheets and NPs deform simultaneously and stress is evenly distributed throughout the system as shown in Fig. 2b. To further elaborate this, we evaluated the maximum strain variation in single layer 3D GrFs contain-NPs system as function of E_f magnitude range i.e. $\sim$10–1000 nN as shown in Fig. 2c. The ε_Δ behavior of 3D GrFs contain-NPs system as function of E_f magnitude for single layer 3D GrFs contain-NPs system is much contrasting. To further elaborate this point precisely, we categorized E_f magnitude in three different ranges, i.e., lower ($E_{fl} \sim$ 10–200 nN), medium ($E_{fm} \sim$ 200–800 nN) and high external field ($E_{fh} \sim$ 800–1000 nN). The 3D GrFs contain-NPs system composed of single layer thick graphene sheets possesses initially increasing trend of strain variation at E_{fl}, followed by the decreasing behavior at E_{fm} and E_{fh}, the critical E_f value beyond which the ε_Δ begins to decrease for single layer thick system is $\sim$200 nN. To further explain the transition of strain variation beyond the critical value, we diminished the graphene sheets to highlight the NPs distribution in single layer 3D GrFs contain-NPs systems as shown in Fig. 2c inset. The NPs remain adsorbed and intact with graphene sheets in single layer thick system and homogenous collapse of single layer 3D GrFs contain-NPs system is particularly observed before critical value. However, we noticed the agglomeration of NPs at the lower fixed boundary in single layer 3D GrFs contain-NPs systems beyond critical value, i.e., in E_{fh} range. The agglomeration of NPs at E_{fh} in single layer 3D GrFs contain-NPs systems occurs due to the flow out of NPs laying on surface of graphene sheets near lower boundary, when subjected to sudden impact generated by E_f. The nanoparticles eventually attract each other to form agglomerates or clusters similar to previously reported results (Khan et al., 2020, 2022, Khan, 2023). Similarly, the four layers thick system also shows similar increasing ε_Δ behavior up to E_{fm} followed by decreasing behavior at E_{fh}. However, the behavior of eight layers thick graphene sheet system is much different, as ε_Δ continuous to increase till E_{fh} with non-homogenous collapses agglomeration of NPs shown in Fig. 2c. The NPs flow out in the direction of applied E_f leaving behind the graphene sheets skeleton even at E_{fl} and E_{fm}, however, this phenomenon is exponentially pronounced particularly at E_{fh} ($\sim$1000 nN).

The microstructural evolution of single- and eight-layers thick

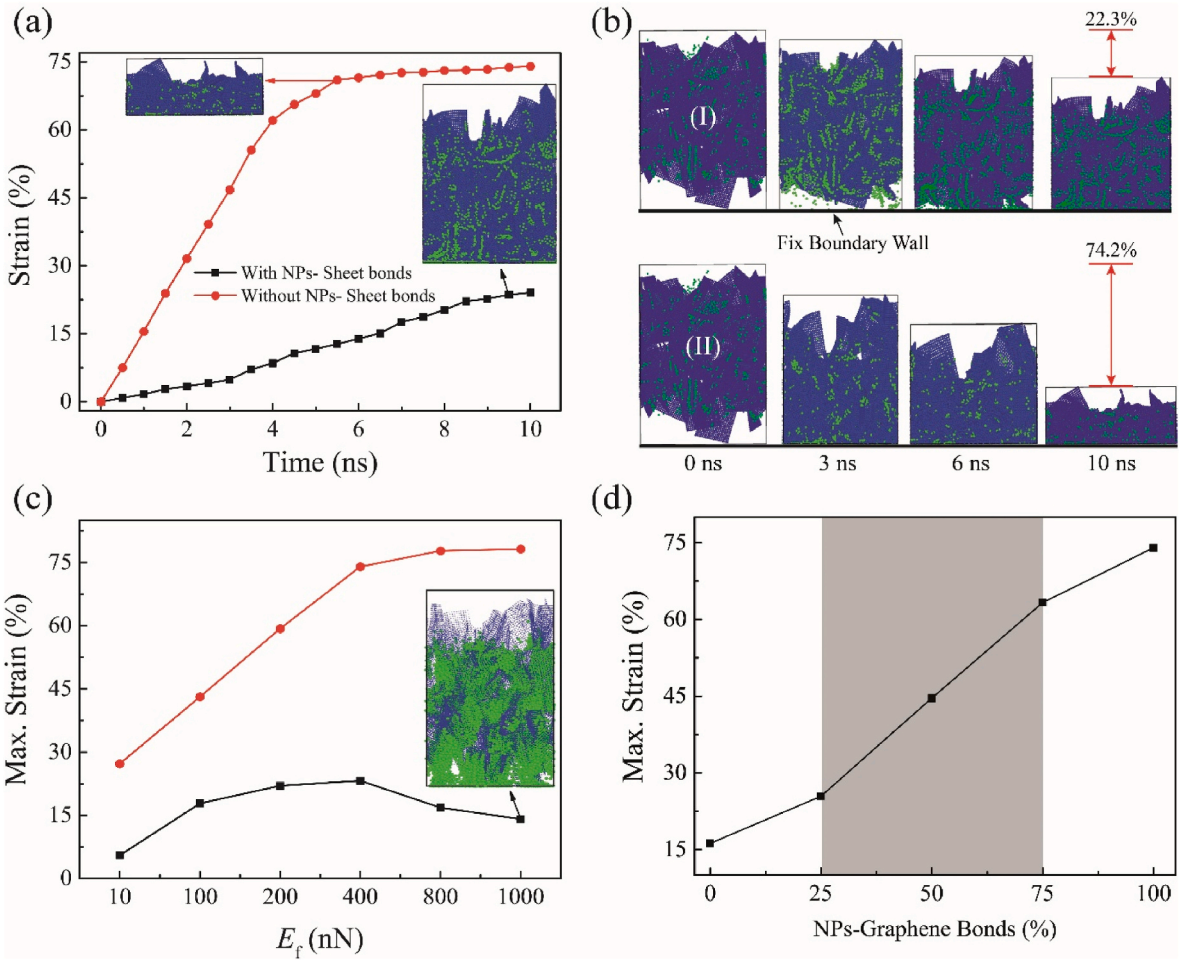

Fig. 4. Strain variation and deformation behavior of 3D GrFs contain-NPs system; (a) Strain variation (ε_Δ) with respect to time as function of crosslinks in 3D GrFs contain-NPs systems; (b) Microstructural deformation of two cases of GrFs contain-NPs at $E_f \sim 400$n; (I) The system with Gra-Gra bond deform up to ~22.3%, (II) The system with NPs-Gra & Gra-Gra bond deform up to ~74.2% respectively; (c) Maximum strain sensitivity as function of E_f magnitudes at varying crosslinks in 3D GrFs contain-NPs systems; (d) The strain variation of case (II) GrFs contain-NPs system as function of NPs and graphene bonds density.

graphene sheet systems under E_f is elaborated in Fig. 3. We observe the phenomenon of wrapping of thin graphene sheets (single layer) around NPs (See movie M1). Furthermore, in case of thick graphene sheets (eight layers) we observe the movement of NPs on surface of graphene sheets and jump of NPs from one (pink) to another (red) graphene sheet (See movie M2 and M3) as shown in Fig. 3. It is evident that in-plane stiffness of single layer graphene sheets is much less relative to multi layered graphene sheets (Kordkheili and Moshrefzadeh-Sani, 2013). So, the thin or single layer graphene sheets can easily wrap, deform or twist when subjected to external stimuli. Similar wrapping of single layer graphene sheets around NPs is observed in our numerical experiments as shown in Fig. 3a. This wrapping phenomenon of single layer sheets around NPs is perfectly aligned with experimental results (Wang et al., 2020), that quote the wrapping of nano balls around thin graphene sheets as elaborated in Fig. 3a. (Wei et al., 2013). However, it is obvious that eight-layer thick graphene sheet owns high in-plane strength and stiffness, that eventually resists the bending or deformation of graphene sheets, when subjected to E_f. Hence, the negligible bending of thick sheets is observed in our numerical experiments. The NPs experiencing E_f stimuli initially move on the surface of graphene sheets and then eventually migrate out into pores as shown in Fig. 3b-I. Furthermore, we also observed the jump of NPs from one sheet to another sheet and finally flow out of NPs into the pores as highlighted in Fig. 3(c-II). The movement of NPs on graphene sheets is much similar to experimentally observed migration phenomenon of Pd NPs on exfoliated graphene sheets actuated by thermal gradient as function of time (Jin et al., 2010). The deformation behavior of four layers thick 3D GrFs contain-NPs system is mostly dominated by bending of sheets followed by migration of NPs into the pores. It is obvious that 3D GrFs contain-NPs systems composed of thin graphene sheets exhibit high ε_Δ comparative to thick graphene sheets systems, which resist the bending and deformation when subjected to E_f. These findings can be helpful in design of futuristic ultra-sensitive sensors.

3.2. *Effect of crosslinks and recovery behavior of GrFs contain-NPs*

Owing to the effect of layers thickness on deformation of non-bonded 3D GrFs contain-NPs system under E_f., we particularly opted the single layer thick system to further study the effect of crosslinks on deformation behavior and strain variation of 3D GrFs contain-NPs system. We evaluated the two different cases of crosslinks at $E_f \sim 400$ nN and $V_f \sim 3\%$; (I) Gra-Gra bond, i.e., system having bonds between graphene sheets only, (II) NPs-Gra & Gra-Gra bond, i.e., the system having bonds both between nanoparticles-graphene sheets and graphene-graphene sheets. The ε_Δ of two cases as function of crosslinks at $E_f \sim 400$ nN is depicted in Fig. 4a. We found that ε_Δ of 3D GrFs contain-NPs system is much influenced by the addition of crosslinks. The addition of crosslinks between graphene sheets only improved the ε_Δ to ~22.3%. Furthermore, if nanoparticles-graphene sheets and graphene-graphene sheets both are bonded, the colossal improvement in ε_Δ of 3D GrF contain-NPs

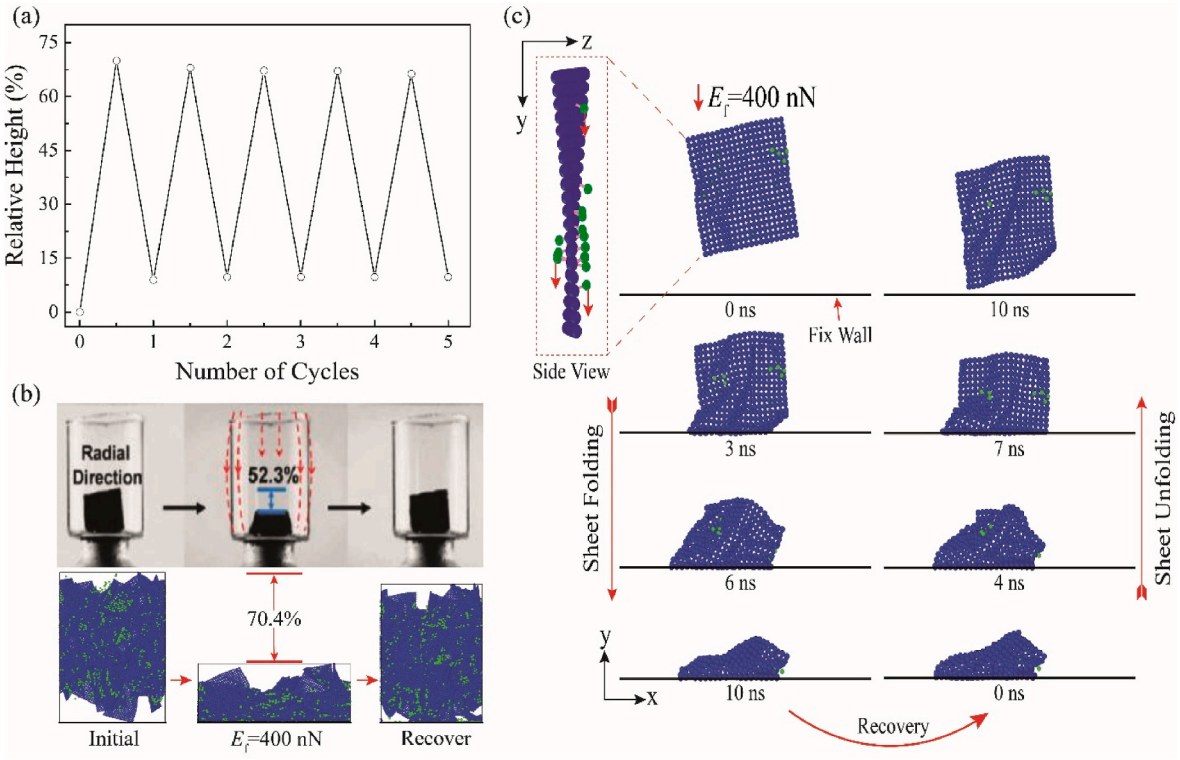

Fig. 5. Microstructural deformation of GrFs contain-NPs; (a) Recovery behavior of NPs-Gra & Gra-Gra bonded 3D GrFs contain- NPs at E_f ~400 nN for five cyclic loadings; (b) Comparison of our numerical experimental results of NPs-Gra & Gra-Gra bonded 3D GrFs contain- NPs system to reported experimental results under magnetic field (Xu et al., 2015b); (c) The folding and unfolding of four layer graphene sheet actuated by directional motion of bonded NPs (shown in side view) under applied external field (E_f~400 nN).

system is found, i.e., ~74.2% at E_f~400 nN as shown in Fig. 4a. The effect of crosslinks effects on ε_Δ can further be intricate through microstructural evolution. The strain variation and microstructural deformation of both cases when subjected to E_f~ 400 nN has been demonstrated in Fig. 4b. We observed that in case (I) the non-bonded adsorbed particles come out of graphene sheets skeleton to agglomerate at the fix wall boundary. This effect is more pronounced at E_{fh} range that lead to lower ε_Δ of systems. However, addition of crosslinks between nanoparticle-graphene sheets significantly can enhance the ε_Δ and impart homogenous deformation of GrF contain-NPs system as shown in Fig. 4b (II). We further evaluated the crosslinks effect on ε_Δ as function of E_f magnitude as shown in Fig. 4c. The case (I) Gra-Gra bond depicts similar trend of increase in ε_Δ of 3D GrFs contain-NPs system from E_{fl} to E_{fm} followed by the decreasing behavior beyond E_{fm} up to E_{fh} as shown in Fig. 4c, that is attributed to the drainage of adsorbed nanoparticles to agglomerate at fix boundary when subjected to high magnitude E_f. The case (II) has different trend comparative to case (I). The ε_Δ of case (II) continues to increase with increasing magnitude of E_f and eventually attain the magnetic saturation at E_{fh} similar to experimentally reported results (Xu et al., 2015b). The bonded nanoparticles with graphene sheets ensure the continual dragging of graphene sheets in direction of applied E_f, that eventually causes the increased ε_Δ of overall 3D GrFs contain-NPs system. The graphene sheets are also bonded to each other along with nanoparticles-graphene bond, the deformation mechanism become more homogenous and essence of uniformity in deformation is observed that ultimately increases ε_Δ value as shown in Fig. 4c. We also evaluated the effect of NPs-graphene crosslink density effect on strain variation in case (II). We found that below 25% crosslink density, the effect in strain variation is relatively less, however beyond 25% the strain variation increases exponentially with increase in crosslink density up to 75% as highlighted in Fig. 4d. This can be realized easily that bonded NPs when experiencing external field can effectively deform the system more homogenously comparative to non-bonded adsorbed NPs.

To further investigate the cyclic loading effect, we opted case (II) having layer thickness equal to four. We systematically turn on and off the applied E_f~400 nN for five consecutive cycles and found ~90% recovery of case (II) as depicted in Fig. 5a. The bonded graphene sheets and nanoparticles enables the maximum recovery when E_f is removed. However, the case (I) exhibits poor recovery of ~30%. The recovery behavior of case (II) is much better relative to case (I) where only sheets recovers partially leaving behind the agglomerated nanoparticles stick to fix boundary. The recovery behavior of case (II) is much similar to experimentally reported results as elaborated in Fig. 5b, where magnetic aerogel recovers to original height when magnetic field is removed (Xu et al., 2015b).

We further observe the folding of sheets caused by the bonded NPs, when subjected to E_f as shown in Fig. 5c. The NPs are bonded to both surfaces of graphene sheet as shown in side view of Fig. 5c. When NPs experienced the E_f as indicated by red arrows, the four layers graphene sheet is enforced to pull in the direction of applied E_f, the eventually cause the folding of graphene sheet around fix boundary at 10 ns?as shown in Fig. 5c. When E_f is applied, initially bonded NPs dragged the graphene sheet to fix boundary and finally graphene sheet folds due to continuous force experienced by bonded NPs (See Movie M4). The four layer graphene sheet even at 0 ns is slightly crumpled due to lower in-plane stiffness which is consistent to previously reported results (Liao et al., 2021). We noted that when E_f is removed the four-layer graphene sheet unfold gradually retaining the ~9.6% residual strain at 10 ns?as shown in Fig. 5c (See Movie M5). The unfolding of sheets along with bonded nanoparticles causes the recovery of NPs- Gra bond systems to maximum values. Hence, the crosslink is vital factor to tune the ε_Δ and recovery feature of magnetic aerogels. The experimental reported results as depicted in Fig. 5b was also bonded magnetic aerogel (i.e., NPs-sheet & graphene) that eventually showed the maximum recovery with similar structure similarity (Xu et al., 2015b). In our study the

variation of temperature and air pressure is countered through NPT ensemble. Air may cause a negligible effect on strain variation of magnetic aerogels however dust or pollutants or air moisture (fog) may influence the strain variation of such a heterogeneous system through the possible chemical reaction between nanoparticles and pollutants (Li et al., 2016). These aspects should be investigated separately.

4. Conclusions

In this paper, the strain variation and its microscopic deformation mechanism of graphene foam contained nanoparticles materials under external magnetic field (E_f) are systematically investigated with coarse-grained molecular dynamics simulation method, in which effects of the graphene thickness and crosslinks on the strain variation, recovery behavior and microstructural evolution are considered. The proposed numerical model is in good agreement with the our previously reported model and experimental results.

With the gradual increase of layer thickness from single to eight layers, the microstructural evolution process changes from wrapping of nanoparticles between single layer to flow and jump of nanoparticles from one sheet to another. Furthermore, the strain sensitivity is much influenced by the layer thickness. The single layer thick system exhibits higher strain variation relative to eight layers thick system. We further found the critical values of applied external field magnitude for single ($E_f \sim 200$ nN) layer thick system beyond which the strain sensitivity of system decreases. However, sensitivity continues to increase with increasing E_f magnitude for the eight-layer thick system.

The addition of crosslinks has significant effect on the strain sensitivity of hybrid composite. With the addition of crosslink, homogenous deformation of hybrid composite occurs, yielding improved strain sensitivity of the composite. The NPs-Gra & Gra-Gra bond system recovers to $\sim$90% relative to non-bonded system which recovers to maximum $\sim$30% respectively. The folding and unfolding mechanism of graphene sheet is also observed. The strain sensitivity of hybrid system acquiring crosslinks continues to increase with increasing external field and eventually attains the magnetic saturation level. However, strain sensitivity of non-bonded system finally decreases after critical external field value ($\sim$200 nN). The results in this study should be helpful not only to understand the microscopic deformation mechanism of magnetic aerogel, but also to the design of advanced functional devices by tuning the layer thickness and crosslink variation in nanoparticle-filled foam materials.

Author contributions

M.B·K S·H.C. and C.W. conceived the original idea, designed and supervised the simulations. M.B.K. formulated the numerical model, conducted all simulations and drafted the paper. S.H.C. and C.W. revised the manuscript. All authors reviewed and contributed to the paper.

Notes

The authors declare no competing interest.

Declaration of competing interest

The authors declare that they have no known competing financial interests or personal relationships that could have appeared to influence the work reported in this paper.

Data availability

Data will be made available on request.

Acknowledgements

The work reported here is supported by NSFC through Grants #12032004, #12293002, #11972348, #12002034, Strategic Priority Research Program of the Chinese Academy of Sciences (Grants No. XDB22040503) and the CAS/SAFEA International Partnership Program for Creative Research Teams.

Appendix A. Supplementary data

Supplementary data to this article can be found online at https://doi.org/10.1016/j.mechmat.2023.104752.

References

Brown, G.V., L.J.J.o.A.P. Flax, 1964. Superposition of semi-infinite solenoids for calculating magnetic fields of thick solenoids. Appl. Phys. 35 (6), 1764–1767.
Casu, A., et al., 2007. Magnetic and structural investigation of highly porous CoFe2O4–SiO2 nanocomposite aerogels. Phys. Chem. C 111 (2), 916–922.
Casula, Maria.F., Corrias, A., Paschina, G.J., 2001. Iron oxide–silica aerogel and xerogel nanocomposite materials. Non-Crystalline Solids 293, 25–31.
Chen, Z., et al., 2011. Three-dimensional flexible and conductive interconnected graphene networks grown by chemical vapour deposition. Nat. Mater. 10 (6), 424.
Chen, G., et al., 2014. Fabrication of three-dimensional graphene foam with high electrical conductivity and large adsorption capability. Appl. Surf. Sci. 311, 808–815.
Chen, X., et al., 2020. Fabrication of superelastic and highly conductive graphene aerogels by precisely "unlocking" the oxygenated groups on graphene oxide sheets. Carbon 162, 552–561.
Cranford, S., Buehler, M.J., 2011. Twisted and coiled ultralong multilayer graphene ribbons. Model. Simulat. Mater. Sci. Eng. 19 (5), 054003.
Dienwiebel, M., et al., 2004. Superlubricity of graphite. Phys. Rev. Lett. 92 (12), 126101.
Gao, W., Wang, X.J.P.T., 2019. Magneto-elastic properties of isotropic MR elastomers with a tri-modal particle size distribution. Polym. Test. 80, 106105.
Gu, S., Zhu, A., 2020. Graphene nanosheets loaded Fe3O4 nanoparticles as a promising anode material for lithium ion batteries. J. Alloys Compd. 813, 152160.
Huang, L., et al., 2015. Multifunctional graphene sensors for magnetic and hydrogen detection. ACS Appl. Mater. Interfaces 7 (18), 9581–9588.
Jin, Z., et al., 2010. Decoration, migration, and aggregation of palladium nanoparticles on graphene sheets. Chem. Mater. 22 (20), 5695–5699.
Kang, W., et al., 2020. A novel robust adsorbent for efficient oil/water separation: magnetic carbon nanospheres/graphene composite aerogel. J. Hazard Mater. 392, 122499.
Khan, M.B., et al., 2020. The mechanical property and microscopic deformation mechanism of nanoparticle-contained graphene foam materials under uniaxial compression. Nanotechnology 32 (11), 115701.
Khan, M.B., et al., 2022. The mechanical property and micro-mechanism of nanoparticle-contained graphene foam materials under uniaxial tension. Comput. Mater. Sci. 206, 111277.
Kharissova, O.V., Dias, H.R., Kharisov, B.I.J.R.a., 2015. Magnetic adsorbents based on micro-and nano-structured materials. RSC Adv. 5 (9), 6695–6719.
Kordkheili, S.H., Moshrefzadeh-Sani, H.J.C.M.S., 2013. Mechanical properties of double-layered graphene sheets. Comput. Mater. Sci. 69, 335–343.
Lee, S.H., Jung, J.H., Oh, I.K.J.S., 2014. 3D networked graphene-ferromagnetic hybrids for fast shape memory polymers with enhanced mechanical stiffness and thermal conductivity. Small 10 (19), 3880–3886.
Li, Z.-D., et al., 2016. Preparation and photocatalytic performance of magnetic Fe3O4@TiO2 core–shell microspheres supported by silica aerogels from industrial fly ash. J. Alloys & Compunds 659, 240–247.
Li, F., et al., 2020a. Functional magnetic graphene composites for biosensing. Molecular Sci 21 (2), 390.
Li, J., et al., 2020b. Three-dimensional macroassembly of hybrid C@ CoFe nanoparticles/reduced graphene oxide nanosheets towards multifunctional foam. Carbon 157, 427–436.
Liao, Y., Li, Z., Xia, W., 2021. Size-dependent structural behaviors of crumpled graphene sheets. Carbon 174, 148–157.
Liu, C., et al., 2015. Versatile fabrication of the magnetic polymer-based graphene foam and applications for oil–water separation. Colloids Surf., A 468, 10–16.
Liu, F., Wang, C., Tang, Q., 2018. Conductivity maximum in 3D graphene foams. Small 14 (32), 1801458.
Nieto, A., Boesl, B., Agarwal, A., 2015. Multi-scale intrinsic deformation mechanisms of 3D graphene foam. Carbon 85, 299–308.
Pan, D., et al., 2017. Graphene foam: uniaxial tension behavior and fracture mode based on a mesoscopic model. ACS Nano 11 (9), 8988–8997.
Pan, D., Wang, C., Wang, X.J.A.n., 2018. Graphene foam: hole-flake network for uniaxial supercompression and recovery behavior. ACS Nano 12 (11), 11491–11502.
Pierre, A.C., Pajonk, G.M.J.C.R., 2002. Chemistry of aerogels and their applications. Chem. Rev. 102 (11), 4243–4266.
Plimpton, S., 1995. Fast parallel algorithms for short–range molecular dynamics. J. Comput. Phys. 117, 1–19.
Samad, Y.A., et al., 2015. Graphene foam developed with a novel two-step technique for low and high strains and pressure-sensing applications. Small 11 (20), 2380–2385.

Shah, N., et al., 2021. Magnetic aerogel: an advanced material of high importance. RSC Adv. 11 (13), 7187–7204.
Shang, J.J., et al., 2018. Compressive deformation mechanism of honeycomb-like graphene aerogels. Carbon 134, 398–410.
Shi, Y., Gao, X., Qiu, J., 2019. Synthesis and strengthened microwave absorption properties of three-dimensional porous Fe3O4/graphene composite foam. J Ceram Int 45 (3), 3126–3132.
Stukowski, A., 2010. Visualization and analysis of atomistic simulation data with OVITO–the Open Visualization Tool. Model. Simulat. Mater. Sci. Eng. 18 (1), 015012.
Suktha, P., et al., 2019. In situ mass change and gas analysis of 3D manganese oxide/graphene aerogel for supercapacitors. RSC Adv. 9 (49), 28569–28575.
Wang, C., Zhang, C., Chen, S., 2016. The microscopic deformation mechanism of 3D graphene foam materials under uniaxial compression. Carbon 109, 666–672.
Wang, C., Pan, D., Chen, S.J.C., 2018a. Energy dissipative mechanism of graphene foam materials. Carbon 132, 641–650.
Wang, Y., et al., 2018b. Fe3O4 nanoparticle/graphene aerogel composite with enhanced lithium storage performance. Appl. Surf. Sci. 458, 1035–1042.
Wang, C., Zhang, C., Chen, S.J.C., 2019a. Micro-mechanism and influencing factors of graphene foam elasticity. Carbon 148, 267–276.
Wang, C., Zhang, C., Chen, S.J.C., 2019b. Micro-mechanism and influencing factors of graphene foam elasticity. Carbon 148, 267–276.
Wang, X., et al., 2020. CoFe2O4/N-doped reduced graphene oxide aerogels for high-performance microwave absorption. J. Chem. Eng. 388, 124317.
Wei, D., et al., 2013. Formation of graphene-wrapped nanocrystals at room temperature through the colloidal coagulation effect. Part. Part. Syst. Char. 30 (2), 143–147.
Xu, X., et al., 2015a. Self-sensing, ultralight, and conductive 3D graphene/iron oxide aerogel elastomer deformable in a magnetic field. ACS Nano 9 (4), 3969–3977.
Xu, X., et al., 2015b. Self-sensing, ultralight, and conductive 3D graphene/iron oxide aerogel elastomer deformable in a magnetic field. ACS Nano 9 (4), 3969–3977.
Xu, X., et al., 2019. Three dimensionally free-formable graphene foam with designed structures for energy and environmental applications. ACS Nano 14 (1), 937–947.
Yang, S., et al., 2014. Magnetic graphene foam for efficient adsorption of oil and organic solvents. J. Colliad & Interface Sci 430, 337–344.
Yuan, H., et al., 2020. Graphene oxide decorated with titanium nanoparticles to reinforce the anti-corrosion performance of epoxy coating. Coatings 10 (2), 129.
Zeb, M.H., et al., 2019. Superior magnetoresistance performance of hybrid graphene foam/metal sulfide nanocrystal devices. ACS Appl. Mater. Interfaces 11 (21), 19397–19403.
Zhang, Y., et al., 2020. A flexible non-enzymatic glucose sensor based on copper nanoparticles anchored on laser-induced graphene. Carbon 156, 506–513.
Zhu, S., et al., 2020. Flexible Fe3O4/graphene foam/poly dimethylsiloxane composite for high-performance electromagnetic interference shielding. Composite Sci. & tech. 189, 108012.
Khan, M.B., et al., 2023. Nanoparticles surface energy effect on mechanical properties and microscopic deformation 3D heterogeneous nanostructures. Nano,18 7, 2350–053.